High-Sensitivity Charge Detection with a Single-Lead Quantum Dot for Scalable Quantum Computation

M. G. House, I. Bartlett, P. Pakkiam, M. Koch, E. Peretz, J. van der Heijden, T. Kobayashi, S. Rogge, and M. Y. Simmons

High sensitivity charge detection with a single-lead quantum dot for scalable quantum computation

M. G. House,[1, *] I. Bartlett,[1] P. Pakkiam,[1] M. Koch,[1] E. Peretz,[1]
J. van der Heijden,[1] T. Kobayashi,[1] S. Rogge,[1] and M. Y. Simmons[1]

[1] *Centre of Excellence for Quantum Computation and Communication Technology,
School of Physics, University of New South Wales, Sydney, NSW 2052, Australia*

We report the development of a high sensitivity semiconductor charge sensor based on a quantum dot coupled to a single lead, designed to minimize the geometric requirements of a charge sensor for scalable quantum computing architectures. The quantum dot is fabricated in Si:P using atomic precision lithography and its charge transitions are measured with rf reflectometry. A second quantum dot with two leads placed 42 nm away serves as both a charge for the sensor to measure and as a conventional rf single electron transistor (rf-SET) with which to make a comparison of the charge detection sensitivity. We demonstrate sensitivity equivalent to an integration time of 550 ns to detect a single charge with a signal-to-noise ratio of 1, compared with an integration time of 55 ns for the rf-SET. This level of sensitivity is suitable for fast ($< 15\,\mu$s) single-spin readout in quantum information applications, with a significantly reduced geometric footprint compared to the rf-SET.

I. INTRODUCTION

The spin states of electrons or nuclei in a semiconductor host are important candidates to meet the needs of quantum information processing because they are magnetic in nature and have only weak interactions with their surrounding environment [1–4]. Initialization, control, and readout of single electron spins confined on individual phosphorus donors in isotopically purified ^{28}Si have now been achieved with very high fidelity and coherence times of hundreds of milliseconds [5–7]. P donor devices in Si can be fabricated by scanning tunneling microscope (STM) lithography, which allows placement of single P donors into a Si lattice precise to the atomic scale [8]. Heavily P doped, metallic regions can also be patterned in the same lithographic step and aligned to individual donor sites with nanometer accuracy to form electrical control leads and larger quantum dots. The separation between P atom qubit sites must be $\lesssim 15$ nm to set appropriate tunnel couplings and exchange interactions between them [7, 9]. This requirement puts severe limits on the space available for individual control and readout electrodes if the device is to contain many qubits.

Single electron spin readout in quantum dots and donors is typically performed by spin-to-charge conversion [10]. Charge states are distinguished with a nearby mesoscopic field-effect charge sensor, such as a single electron transistor (SET) [11, 12], quantum point contact [13, 14], or tunnel junction [15]. The SET offers the highest sensitivity demonstrated to date, but it requires at least three electrical contacts to operate: source, drain, and gate. It therefore occupies a large geometric footprint in present devices (see e.g. Ref. 7), which must be minimized for the future development of increasingly complex multi-qubit devices with multiple sensors. An alternative sensing strategy is to measure the susceptibility of a single electron tunneling at radio frequencies, which requires only one terminal to distinguish singlet and triplet spin states on double quantum dots by Pauli blockade, so-called 'gate sensing' [16–20]. Gate sensing cannot directly readout a single electron spin because it induces the electron to tunnel back and forth to a reservoir, destroying the spin state before it can be resolved. Thus there is still a need for a charge sensor which requires minimal wiring and space to enable scalable quantum computing architectures for single-spin qubits. For high fidelity spin readout the charge sensitivity must be good enough to resolve the tunneling event signatures of the excited spin state, which typically occurs on timescales less than 1 ms, with high enough signal-to-noise ratio (SNR) to reliably distinguish them from noise [7, 21]. The charge sensitivity can be stated as an SNR for a given acquisition bandwidth, or equivalently (assuming white noise) the integration time required to resolve a single charge with a specified SNR.

In this work we investigate the use of a single-lead quantum dot (SLQD) as a capacitive charge sensor and how to optimize its sensitivity to make it suitable for real-time spin readout measurements. Although no dc current passes through the quantum dot, its charge transitions can be detected with rf reflectometry, as has been demonstrated with a similar superconducting device called the single-electron box [22]. We show that the SLQD can be used as a capacitive charge sensor when it is tuned to one of its charge transitions where there is reflected signal response. Any motion of a charge on a nearby quantum dot shifts the SLQD electrochemical potential and shuts off the reflected signal response. By measuring the SLQD sensor dot with rf reflectometry only one lead is required, and it can be tuned by a dc voltage supplied through a bias tee. This makes for a compact, tunable charge sensor which is capable of detecting the signature of single-electron spin readout in less than 15 μs.
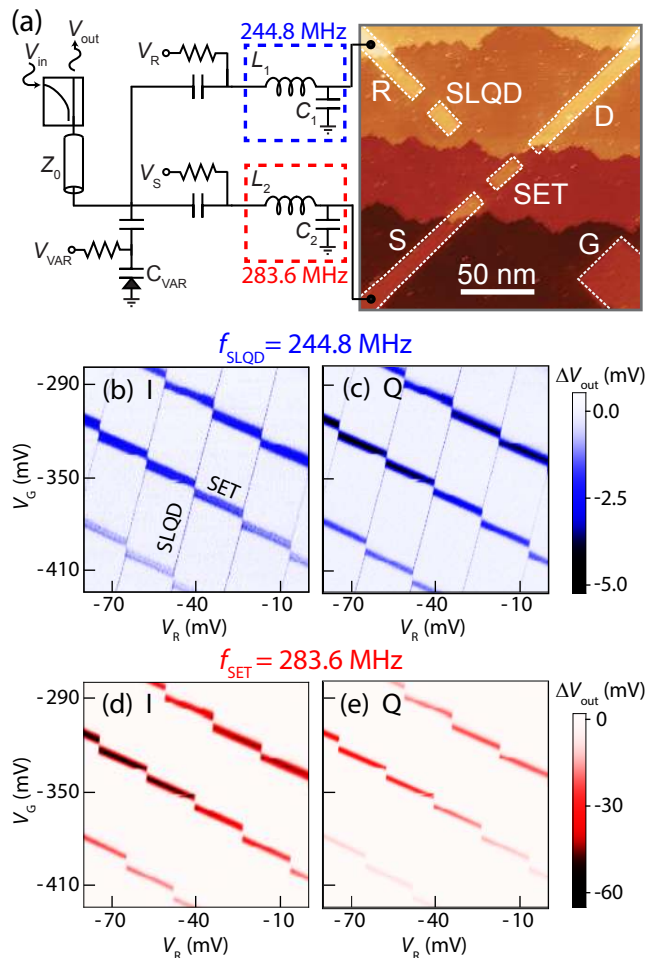
* matthew.house@unsw.edu.au

FIG. 1. **Device geometry, impedance matching circuit, and stability diagrams.** (a) STM image of the device during the lithography process. Lighter colored regions indicate H desorption where the final device is P doped. The device consists of two quantum dots, SLQD and SET. Source (S) and drain (D) leads are tunnel-coupled to the SET, while the SLQD has only a single lead (R). A gate (G) is used to independently tune the SET potential. The rf impedance matching circuit consists of two parallel LC resonances at f_{SLQD} =244.8 MHz connected to R and f_{SET} =283.6 MHz connected to S. (b) In-phase (I) and (c) quadrature (Q) parts of the reflected signal response at f_{SLQD}, which show lines in response to both the SLQD (thin positive-slope lines) and SET (negative slope lines). (d) In-phase (I) and (e) quadrature (Q) parts of the reflected signal response at f_{SET}, which is sensitive only to the SET charge transitions.

II. EXPERIMENT DESIGN

Figure 1(a) presents an STM image of the device lithographic pattern along with a schematic of the rf measurement circuit. The silicon surface in this image has three atomic steps running nearly horizontal which leads to a monotonic change in height of 0.4 nm from the top to the bottom of the image. Lighter colored regions highlighted

with white dashed lines are where the hydrogen mask has been removed. These areas are P doped (2×10^{14} cm^{-2}) and metallic in the final device while darker regions remain insulating at low temperatures. The design consists of an SQLD tunnel coupled to lead R, an SET quantum dot with tunnel coupling to source (S) and drain (D) leads, and an additional gate (G) for tuning the SET potential. The two quantum dots are 42 nm apart, far enough that there is no significant tunnel coupling between them but close enough to be capacitively coupled. This design allows us to use the SLQD to detect charge transitions of the SET, and *vice versa*, to compare directly the charge sensing performance of the SLQD with the more conventional SET.

Leads R and S are each connected to a separate tank circuit with a unique resonant frequency, which allows them to be addressed and measured separately while connected to the same rf measurement chain [23]. The resonant circuit connected to R is formed by a $L_1 = 620$ nH chip inductor, which along with its parasitic capacitance to ground $C_1 \approx 0.68$ pF has a resonant frequency $f_{\mathrm{SLQD}} = 244.8$ MHz and a quality factor $Q \approx 100$. Similarly the circuit connected to S has $L_2 = 470$ nH, $f_{\mathrm{SET}} = 283.6$ MHz, and $Q \approx 45$. The device and matching circuit are mounted in a dilution refrigerator operating at a base mixing chamber temperature $T_{\mathrm{MC}} = 50$ mK unless otherwise specified. Two rf signals at the resonant frequencies of the matching circuits are added with a power combiner at room temperature and transmitted into the circuit via a coaxial waveguide with impedance $Z_0 = 50\,\Omega$. The reflected rf signal is routed by a directional coupler to an amplifier (Caltech CITLF3) at the 4 K stage of the refrigerator. The output is amplified again at room temperature, split into two analysis chains (one for each frequency), then each is separately demodulated to baseband by an IQ mixer (Polyphase AD0105B) and finally acquired digitally. Connected to the resonant circuits is a variable capacitor C_{VAR} (3 of M/A-COM MA46H204-1056 varactor diodes in parallel), designed to tune the input impedance of the resonant circuits by voltage V_{VAR} [24]. However we observed that C_{VAR} did not vary significantly with V_{VAR} at temperatures < 1 K, but behaved as fixed capacitance $C_{\mathrm{V}} \approx 35$ pF. This capacitance increased the quality factor of each resonance and improved the impedance mismatch by about a factor of 3 compared to previous experiments in Refs. 20 and 25. Unlabeled resistors (100 kΩ) and capacitors (1.5 nF) in the circuit schematic form bias tees to allow dc voltages V_{S}, V_{R}, and V_{VAR} to be applied independently.

III. RESULTS

Fig. 1 illustrates the stability diagrams of the two quantum dots as measured simultaneously at f_{SLQD} (b-c) and at f_{SET} (d-e). The reflected signal V_{OUT} is presented in terms of its I (in-phase / real) and Q (quadrature / imaginary) components, after correcting the over-

all phase of each signal to account for line delay so that $Q \approx 0$ in Coulomb blockade regions [26]. This makes changes in the amplitude of the reflected signal appear primarily in the I channel and phase changes appear in the Q channel. Presenting the complex data in Cartesian coordinates rather than as amplitude and phase is better for comparing responses with different input powers, as we discuss below. When measured at f_{SLQD} as shown in Fig. 1(b) and (c), we see the SLQD response as a series of thin lines with positive slope, each one appearing where an electron transition of the SLQD occurs. This differs from typical quantum dot stability diagrams because as V_R is increased the Fermi level of reservoir R is lowered, inducing electrons to tunnel off the SLQD. The SET response is also visible in these plots as the thicker, negative slope lines. These are visible because the SET is indirectly driven by the signal f_{SLQD} on R [27], and is greatly reduced when the rf input signal at f_{SET} is turned off as seen in Fig. 2(a). We note that we would not expect to see such a response for a typical spin readout target since it would have much weaker tunnel coupling to its lead(s). The response when measured at f_{SET} is shown in Fig. 1(d) and (e), where we observe only the charge transitions of the SET appearing as a series of lines with negative slopes on the plots. This channel is not directly sensitive to SLQD charge transitions but they can be inferred from the shifts in the SET transition lines, demonstrating the typical operation of a capacitive radio frequency SET (rf-SET) charge sensor.

Looking at a zoomed-in picture of two points where the SET and SLQD lines cross in Fig. 2(a), we clearly see the charge offset $\Delta V_{\mathrm{R}}^{(\mathrm{M})} = 1.0\,\mathrm{mV}$ that one electron added to the SET induces on the SLQD. As this charge offset is greater than the SLQD transition linewidth, we can detect the presence or absence of a charge on the SET dot by the position of the SLQD response line alone, demonstrating that the SLQD measured with rf reflectometry can serve as a capacitive charge sensor in the same mode of operation as an rf-SET.

Also in Fig. 2(a) we see a finite response at the "interdot" transition lines, such as between (N+1, M) and (N, M+1). This should not be interpreted as electrons tunneling between the two dots, because the distance between them (42 nm) is too large and no dc current was observed to flow between R and S/D unless a large bias $|V_{\mathrm{R}}| > 0.8\,\mathrm{V}$ was applied. Instead, on this line each cycle of the rf signal pushes an electron on (off) the SLQD, then Coulomb repulsion pushes an electron off (on) the SET, resulting in a net rf current through the device from R to S/D although no electrons transfer between the two quantum dots.

Since the SLQD has only one lead, its capacitive lever arms and charging energies cannot be determined with a Coulomb diamond measurement [3]. Instead we determine the energy scaling from the change in the SLQD peak width with increasing temperature. Fig. 2(b) shows several traces of one SLQD response peak at various mixing chamber temperatures T_{MC} of the refrigerator,
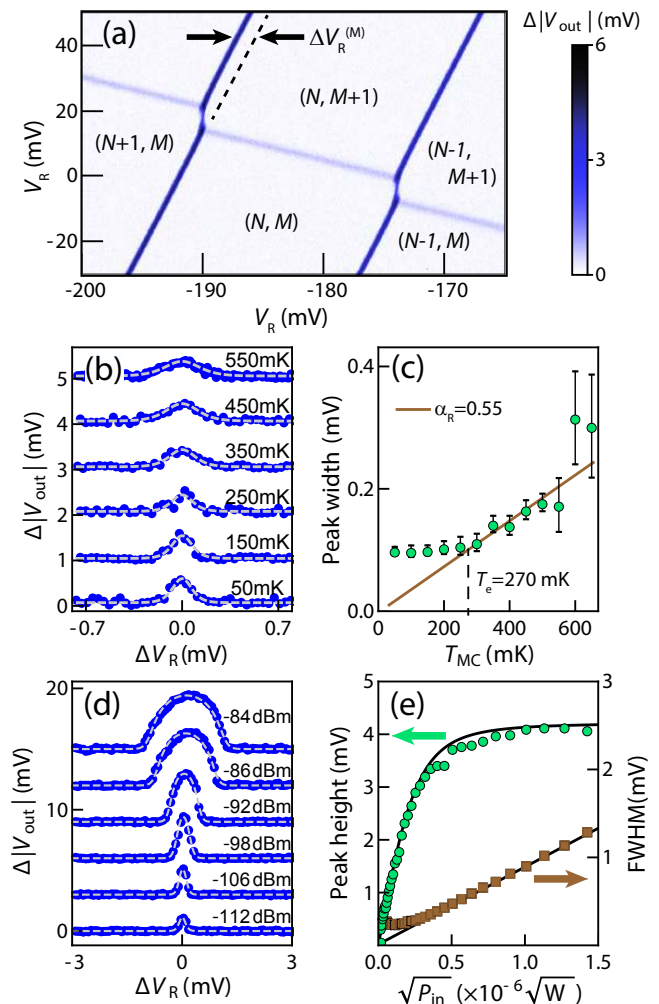

FIG. 2. **SLQD response characterization** (a) Stability diagram measured at f_{SLQD} zoomed in on two crossing points between SLQD and SET charge transitions. (N, M) indicates a region with N electrons on the SLQD and M on the SET. (b) Reflected signal voltage response ($|\Delta V_{\mathrm{out}}|$) profiles of one SLQD peak for various temperatures of the mixing chamber. Each curve is offset by 1 mV for clarity. Dashed lines are fits to a rate equation model for the rf response. (c) Fitted width of an SLQD peak as a function of mixing chamber temperature, which allows us to calibrate the lever arm $\alpha_{\mathrm{R}} = 0.55$ and base electron temperature $T_{\mathrm{e}} \leq 270\,\mathrm{mK}$. (d) SLQD peak profiles for various rf input powers P_{in}. Each curve is offset by 3 mV for clarity. (e) The amplitude (green) and full-width half-maximum (brown) of the SLQD peak as a function of the input signal amplitude.

with the applied power incident at the LC circuits $P_{\mathrm{in}} \approx -125\,\mathrm{dBm}$ small enough to avoid broadening the peak. The peak shape reduces in amplitude and broadens with increasing temperature according to the the quantum capacitance of the transition,

$$C_{\mathrm{q}} = \frac{(1-\alpha_{\mathrm{R}})^2 e^2}{4 k_{\mathrm{B}} T_{\mathrm{e}}} \cosh^{-2}\left[\frac{e(1-\alpha_{\mathrm{R}})\Delta V_{\mathrm{R}}}{2 k_{\mathrm{B}} T_{\mathrm{e}}}\right], \quad (1)$$

where α_R is the capacitive lever arm of the reservoir to the SLQD, T_e is the electron temperature in the reservoir, and ΔV_R is the reservoir voltage relative to the middle of the charge transition [28]. Fitting this function to each of the peaks and plotting the peak width against T_{MC} as shown in Fig. 2(c) we see that the relationship is approximately linear at high T_{MC} where the electrons in the reservoir are well thermalized with the mixing chamber, although there are large uncertainties at the highest temperatures due to the decreased magnitude of the peaks. The slope of the brown line corresponds to $2k_B/e(1-\alpha_R)$, from which we extract the lever arm value $\alpha_R = 0.55$. With this scaling we determine the charging energy of the SLQD, 8.8 meV, and the mutual charging energy between the two quantum dots, $E^{(M)} = (1 - \alpha_R)\Delta V_R^{(M)} = 0.45$ meV, from the charge stability diagrams [29]. At low T_{MC} the peak width saturates to a constant value which suggests that the base electron temperature in this experiment is $T_e \leq 270$ mK. Putting these numbers into Eq. (1) we estimate the quantum capacitance to be $C_q = 0.36$ fF. Because C_q is proportional to $(1 - \alpha_R)^2$ we could significantly increase it by redesigning the device geometry to reduce α_R.

To maximize the strength of the charge detection signal we investigate how the SLQD reflected signal response varies with the rf input power P_{in} as shown in Figure 2(d). We fit these peaks to the shapes predicted by the rate equation model used in Ref. 22, which we solved numerically in order to fully account for the nonlinearities in the tunnel rates. The fitted magnitude and full-width half-maximum (FWHM) values of the peaks are plotted in Fig. 2(e) as a function of the input signal amplitude ($\propto \sqrt{P_{in}}$). For small input amplitudes the magnitude of the response increases linearly and the width of the peak is constant, both of which are described by Eq. (1). At higher input amplitudes the magnitude of the peak saturates to a constant value and the width of the peak increases linearly. In this regime the rf driving amplitude on lead R, V_R^{rf}, is greater than the transition linewidth, $\sim 2k_B T_e/(1 - \alpha_R)e$. A full charge e is transferred on and off of the SLQD each rf cycle and a total ac current $2\pi f_{SLQD}(1-\alpha_R)e$ flows through the device, independent of the driving amplitude. The current cannot increase further unless the driving amplitude is large enough to overcome Coulomb blockade and transfer a second electron to the quantum dot.

The increasing peak width at high input power in Fig. 2(e) gives us a direct calibration of V_R^{rf} as a function of P_{in}. Putting V_R^{rf} and the quantum admittance $i\omega C_q$ into the circuit model we estimate the unamplified reflected signal magnitude in the low power regime. Comparing this result with ΔV_{out} measured after amplification we calibrate the total gain of our amplifier chain to be 88.7 dB, which is within 1 dB of the gains and losses in the chain when measured at room temperature. The calibrated gain in turn allows us to estimate the overall noise temperature of the measurements to be 12 ± 2 K. As this is significantly higher than the rated noise temper-
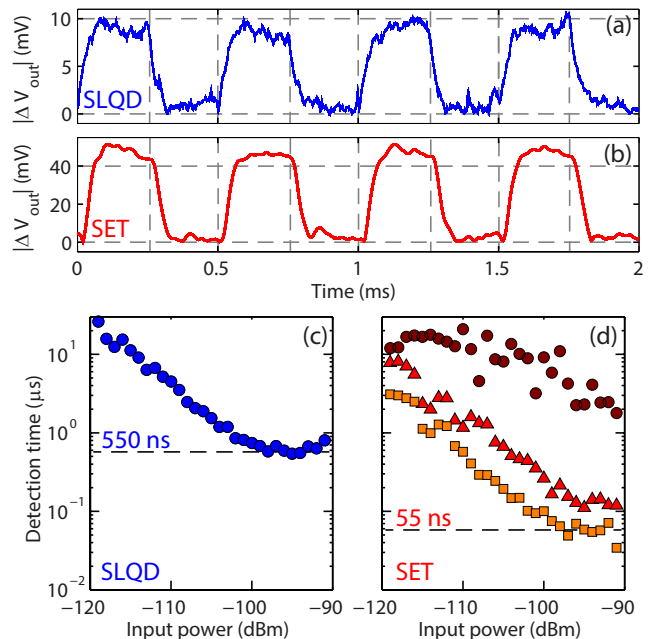

FIG. 3. **Comparison of SLQD and SET real-time signal detection sensitivities.** (a) Real-time data trace of the rf response of the SLQD (blue) taken while applying a 7 mVpp, 2 kHz square wave pulse train to G. Data were digitally filtered to 37.5 kHz bandwidth. (b) Similar data trace measured with the SET (red) with dc bias $V_S = 4$ mV. The SET response is larger due to its smaller impedance. (c) Detection time required for a SNR of 1 for the SLQD charge sensor as a function of the rf input power. The best detection time, 550 ns, was achieved with $P_{in} = -95$ dBm. (d) Detection time for the SET with bias $V_S = 0$ mV (circles), $V_S = 2$ mV (triangles), and $V_S = 4$ mV (squares). The best detection time of about 55 ns was for $V_S = 4$ mV and $P_{in} = -90$ dBm.

ature of the first-stage amplifier (≈ 4 K), the noise level in this experiment may be limited by technical noise or signal losses that occur before the first-stage amplifier, and could be improved in future experiments.

Previous reports have stated that the dispersive response of a quantum dot decreases with increasing input power [30], but this only appeared to be true because the response was interpreted as a phase shift. We observe that the transverse voltage response ΔQ becomes constant at high power but the absolute reflected amplitude $|V_{out}|$ keeps increasing, which means the change in phase $\Delta\phi = \arctan[\Delta Q/|V_{out}|]$ becomes smaller. Nevertheless the voltage noise is constant with increasing signal amplitude, while the phase noise decreases. We conclude that to maximize the SNR of a single-charge detection on a quantum dot capacitively coupled to the SLQD we should chose P_{in} such that we are in the saturation regime, provided that the power broadening of the peak remains less than the charge offset $\Delta V_R^{(M)}$.

To characterize the real-time charge detection sensitivity of the SLQD we acquire time sequence data while tuning V_R and V_G onto an SLQD peak and then applying

a 2 kHz square pulse train of amplitude $\Delta V_G^{(M)} = 7\,\mathrm{mVpp}$ to G. This shifts the potential of the SLQD by the same amount as a charge added to the SET. The SLQD response to this pulse, with (optimized) input power $P_\mathrm{in} = -95\,\mathrm{dBm}$ and filtered to 37.5 kHz bandwidth, is shown in Fig. 3(a). Defining the power SNR as the ratio of the square of the difference in mean signal levels between each phase of pulse to the noise variance we measure an SNR of 50. From this we extrapolate an integration time of about 550 ns required for an SNR of 1. This sensitivity is similar to the best reported for rf quantum point contacts in single-shot spin detection experiments [14]. As expected this detection time decreases with increasing P_in before leveling off, as shown in Fig. 3(c). Above P_in =-95 dBm the detection time increases as the transition peak is broadened to wider than $\Delta V_G^{(M)}$ and the contrast between the two levels is reduced.

For comparison we show a similarly optimized trace taken with the rf-SET in Fig. 3(b), which has an SNR of 500. Here we have applied a dc bias $V_S = 4\,\mathrm{mV}$ to decrease the differential resistance of the SET (to 300 kΩ from 5 MΩ at $V_S = 0\,\mathrm{V}$). The SET measurement has the same noise level but has a larger signal since the impedance of the SET is smaller than that of the SLQD ($\approx 2\,\mathrm{M\Omega}$ imaginary) and therefore for the same driving voltage more power is transferred. The SET detection times for an SNR of 1 as a function of input power and dc bias V_S are shown in Fig. 3(d). For optimal settings $P_\mathrm{in} = -90\,\mathrm{dBm}$ and dc bias $V_S = 4\,\mathrm{mV}$ the detection time is about 55 ns for a SNR of 1.

IV. DISCUSSION

In conclusion, we demonstrated the use of a single-lead quantum dot measured with rf reflectometry as a capacitive charge sensor with tunability and sensitivity suitable for single-spin readout by spin-to-charge conversion. We demonstrated that the detection sensitivity depends upon the input signal level, which plateaus for high input power. The best sensitivity achieved in this experiment enables an SLQD detection time of 550 ns for a SNR of 1, compared to 55 ns with the rf-SET. Assuming we need SNR $\gtrsim 25$ for high-fidelity spin readout, we can achieve it with an integration time of less than 15 μs with this level of sensitivity. While the rf-SET has better sensitivity due to its lower impedance and correspondingly higher signal level, it requires more space and leads in the device. The size of the SLQD in this experiment (21.5 nm × 8.4 nm, about 400 P atoms and electrons) is somewhat arbitrary since the rf response depends on only one tunneling electron at a time, not the charging energy or absolute number of electrons on the SLQD. In principle it could be as small as a single P atom coupled to a single lead a few nanometers wide. The SLQD sensitivity can be improved in future experiments by better impedance matching, designing the device geometry to minimize the SLQD lever arm α_R, and by lowering the noise level in the amplifier chain. The sensitivity of the dispersively measured SLQD may ultimately exceed that of an rf-SET since the latter is fundamentally limited by shot noise [11], while the former is not [31]. Such superior performance may be realizable using a cryogenic parametric amplifier, which has demonstrated dispersive readout detection times less than one microsecond with high SNR [26]. The SLQD is therefore a promising alternative to the SET for detecting single charges and measuring single spins in scalable quantum computing architectures where it is difficult or impossible to integrate the larger SET.

V. ACKNOWLEDGEMENT

[1] B. E. Kane, "A silicon-based nuclear spin quantum computer," Nature **393**, 133–137 (1998).

[2] Daniel Loss and David P. DiVincenzo, "Quantum computation with quantum dots," Phys. Rev. A **57**, 120–126 (1998).

[3] R. Hanson, L. P. Kouwenhoven, J. R. Petta, S. Tarucha, and L. M. K. Vandersypen, "Spins in few-electron quantum dots," Rev. Mod. Phys. **79**, 1217–1265 (2007).

[4] F. A. Zwanenburg, A. S. Dzurak, A. Morello, M. Y. Simmons, L. C. L. Hollenberg, G. Klimeck, S. Rogge, S. N. Coppersmith, and M. A. Eriksson, "Silicon quantum electronics," Rev. Mod. Phys. **85**, 961–1019 (2013).

[5] J. T. Muhonen, J. P. Dehollain, A. Laucht, F. E. Hudson, R. Kalra, T. Sekiguchi, K. M. Itoh, D. N. Jamieson, J. C. McCallum, A. S. Dzurak, and A. Morello, "Storing quantum information for 30 seconds in a nanoelectronic device," Nat. Nanotech. **9**, 986–991 (2014).

[6] J T Muhonen, A Laucht, S Simmons, J P Dehollain, R Kalra, F E Hudson, S Freer, K M Itoh, D N Jamieson, J C McCallum, A S Dzurak, and A Morello, "Quantifying the quantum gate fidelity of single-atom spin qubits in silicon by randomized benchmarking," Journal of Physics: Condensed Matter **27**, 154205 (2015).

[7] T. F. Watson, B. Weber, M. G. House, H. Buch, and M. Y. Simmons, "High-fidelity rapid initialization and

read-out of an electron spin via the single donor d^{-1} charge state," Phys. Rev. Lett. **115**, 166806 (2015).

[8] M. Fuechsle, J. A. Miwa, S. Mahapatra, H. Ryu, S. Lee, O. Warschkow, L. C. L. Hollenberg, G. Klimeck, and M. Y. Simmons, "A single-atom transistor," Nat. Nanotechnol. **7**, 242–246 (2012).

[9] B. Koiller, X. Hu, and S. Das Sarma, Phys. Rev. Lett. **88**, 027903 (2001).

[10] J. M. Elzerman, R. Hanson, L. H. Willems van Beveren, L. M. K. Vandersypen, and L. P. Kouwenhoven, "Single-shot read-out of an individual electron spin in a quantum dot," Nature **430**, 431–435 (2004).

[11] M. H. Devoret and R. J. Schoelkopf, "Amplifying quantum signals with the single-electron transistor," Nature **406**, 1039–1046 (2000).

[12] C. Barthel, M. Kjaergaard, J. Medford, M. Stopa, C. M. Marcus, M. P. Hanson, and A. C. Gossard, "Fast sensing of double-dot charge arrangement and spin state with a radio-frequency sensor quantum dot," Phys. Rev. B **81**, 161308(R) (2010).

[13] M. Field, C. G. Smith, M. Pepper, D. A. Ritchie, J. E. F. Frost, G. A. C. Jones, and D. G. Hasko, "Measurements of coulomb blockade with a noninvasive voltage probe," Phys. Rev. Lett. **70**, 1311–1314 (1993).

[14] C. Barthel, D. J. Reilly, C. M. Marcus, M. P. Hanson, and A. C. Gossard, "Rapid single-shot measurement of a singlet-triplet qubit," Phys. Rev. Lett. **103**, 160503 (2009).

[15] M. G. House, E. Peretz, J. G. Keizer, S. J. Hile, and M. Y. Simmons, "Single-charge detection by an atomic precision tunnel junction," Appl. Phys. Lett. **104**, 113111 (2014).

[16] K. D. Petersson, C. G. Smith, D. Anderson, P. Atkinson, G. A. C. Jones, and D. A. Ritchie, "Charge and spin state readout of a double quantum dot coupled to a resonator," Nano Letters **10**, 2789–2793 (2010).

[17] M. D. Schroer, M. Jung, K. D. Petersson, and J. R. Petta, "Radio frequency charge parity meter," Phys. Rev. Lett. **109**, 166804 (2012).

[18] A. C. Betz, R. Wacquez, M. Vinet, X. Jehl, A. L. Saraiva, M. Sanquer, A. J. Ferguson, and M. F. Gonzalez-Zalba, "Dispersively detected pauli spin-blockade in a silicon nanowire field-effect transistor," Nano Lett. **15**, 4622–4627 (2015).

[19] M. Urdampilleta, A. Chatterjee, C. C. Lo, T. Kobayashi, J. Mansir, S. Barraud, A. C. Betz, S. Rogge, M. F Gonzalez-Zalba, and J. J. L. Morton, "Charge dynamics and spin blockade in a hybrid double quantum dot in silicon," Phys. Rev. X **5**, 031024 (2015).

[20] M. G. House, T. Kobayashi, B. Weber, S. J. Hile, T. F. Watson, J. van der Heijden, S. Rogge, and M. Y. Simmons, "Radio frequency measurements of tunnel couplings and singlet-triplet spin states in si:p quantum dots," Nat. Commun. **6**, 8848 (2015).

[21] A. Morello, J. J. Pla, F. A. Zwanenburg, K. W. Chan, K. Y. Tan, H. Huebl, M. Mottonen, C. D. Nugroho, C. Yang, J. A. van Donkelaar, A. D. C. Alves, D. N. Jamieson, C. C. Escott, L. C. L. Hollenberg, R. G. Clark, and A. S. Dzurak, "Single-shot readout of an electron spin in silicon," Nature **467**, 687–691 (2010).

[22] F. Persson, C. M. Wilson, M. Sandberg, G. Johansson, and P. Delsing, Nano Lett. **10**, 953–957 (2010).

[23] J. M. Hornibrook, J. I. Colless, A. C. Mahoney, X. G. Croot, S. Blanvillain, A. C. Gossard, and D. J. Reilly, Appl. Phys. Lett. **104**, 103108 (2014).

[24] N. Ares, F. J. Schupp, A. Mavalankar, G. Rogers, J. Griffiths, G. A. C. Jones, I. Farrer, D. A. Ritchie, C. G. Smith, A. Cottet, G. A. D. Briggs, and E. A. Laird, Phys. Rev. Applied **5**, 034011 (2016).

[25] S. J. Hile, M. G. House, E. Peretz, J. Verduijn, D. Widmann, T. Kobayashi, S. Rogge, and M. Y. Simmons, "Radio frequency reflectometry and charge sensing of a precision placed donor in silicon." Appl. Phys. Lett. **107**, 093504 (2015).

[26] J. Stehlik, Y.-Y. Liu, C. M. Quintana, C. Eichler, T. R. Hartke, and J. R. Petta, "Fast charge sensing of a cavity-coupled double quantum dot using a josephson parametric amplifier," Phys. Rev. Applied **4**, 014018 (2015).

[27] C. Ciccarelli and A. J. Ferguson, "Impedance of the single-electron transistor at radio-frequencies," New J. Phys. **13**, 093015 (2011).

[28] A. Cottet, C. Mora, and T. Kontos, "Mesoscopic admittance of a double quantum dot," Phys. Rev. B **83**, 121311(R) (2011).

[29] W. G. van der Wiel, S. De Franceschi, J. M. Elzerman, T. Fujisawa, S. Tarucha, and L. P. Kouwenhoven, "Electron transport through double quantum dots," Rev. Mod. Phys. **75**, 1–22 (2002).

[30] J. I. Colless, A. C. Mahoney, J. M. Hornibrook, A. C. Doherty, H. Lu, A. C. Gossard, and D. J. Reilly, "Dispersive readout of a few-electron double quantum dot with fast rf gate sensors," Phys. Rev. Lett. **110**, 046805 (2013).

[31] M. F. Gonzalez-Zalba, S. Barraud, A. J. Ferguson, and A.C. Betz, "Probing the limits of gate-based charge sensing," Nat. Commun. **6**, 6084 (2015).